

Tuned POD Galerkin models for transient feedback regulation of the cylinder wake

Mark Luchtenburg* and Gilead Tadmor†

*Communication & Digital Signal Processing Center,
Northeastern University, 440 Dana Research Building, Boston, MA 02115, U.S.A.*

Oliver Lehmann‡, Bernd R. Noack§ and Rudibert King¶

Sfb557, Technical University of Berlin, Straße des 17. Juni, 10623 Berlin, Germany

Marek Morzyński||

*Institute of Combustion Engines and Transportation,
Poznan University of Technology, Piotrowo 3, 60-965 Poznan, Poland*

Proper orthogonal decomposition (POD) Galerkin models are typically obtained from a single reference, such as an attractor. The POD model provides a very efficient representation of the reference but is often incapable to handle transient dynamics and other changes in flow conditions. These shortcomings are detrimental in feedback flow control applications. A novel concept of *tuned Galerkin models* is suggested, by which the global model interpolates a succession of similar-structure local models. The tuned model covers a controlled transient manifold, compensating for the gradual deformation of dominant flow structures, along such transients. The model is an enabler for both improved tracking performance, as well as for optimized control hardware placement, taking into account the entire dynamic range of interest. These concepts are demonstrated in the benchmark of stabilization of the wake flow behind a circular cylinder.

I. Introduction

This paper is part of a continued effort (see e.g.,^{?,1,2,4-11}) to develop low order flow models that can be used for feedback design. Such models need to strike a difficult balance between the complexity entailed by a rich dynamic envelope, covering relevant transients, and the simplicity and low dimension necessary for implementable design. Proper orthogonal decomposition Galerkin models (GMs)¹² provide efficient Karhunen-Loève approximation of flow data, but their typical dynamic fragility away from the reference orbit and flow conditions is particularly detrimental for control design, where transients representation is essential.

A key challenge for the representation of transient dynamics, away from a single reference orbit, is that dominant flow structures tend to change significantly as the system traverses such trajectories. Referring to the driving example of this paper, the 2D laminar cylinder wake, characteristics of such changes include a substantial shortening of the recirculation bubble of the mean flow, and shorter vortex shedding periods and spatial wave length of the von Karman vortices, as the system transition from the unstable steady flow to the natural vortex shedding limit cycle.¹³ A second challenge is due to the generation of flow structures

*Doctoral student, visiting from TUB

†Professor, CDSP Director

‡Diplom Student

§Junior Professor

¶Professor and Sfb 557 Director

||Professor

Copyright © 2006 by M. Luchtenburg, G. Tadmor, O. Lehmann, B.R. Noack, R. King and M. Morzyński. Published by the American Institute of Aeronautics and Astronautics, Inc. with permission.

that are not present in the natural flow by the actuation, especially under higher gains. This is reflected by the need to include up to 40 modes in a Galerkin model used for optimal control of this system,⁹ whereas only 3 modes suffice for a decent representation of natural transients.⁷

This note aims to regain low dimension in design oriented flow models without losing the necessary dynamic range. It exploits the fact that while undergoing continuous deformations, the POD model at intermediate (natural or controlled) attractors often maintains both the same small number of leading modes, their main topological features and key dynamic properties of the local Galerkin system ODE. We shall therefore pursue a novel idea of *tunable models*: The tuning parameter in such models reflects slow dynamics, such as changes in the mean flow, and is used to adjust the expansion modes and model coefficients of faster, local dynamics, such as periodic vortex shedding. The interpretation of the state of the Galerkin system as a vector of Fourier coefficients of a fixed set of expansion modes will thus be adjusted as the system traverses transient trajectories and moves from the domain of one local model to the next. This framework lends itself as a means to maintain high model fidelity along transients by allowing the Galerkin system to benefit from a large number (ideally, a continuum) of expansion modes, while maintaining a local low order. In the cylinder wake example, instead of using 40 expansion modes we would suggest multiple mode pairs, each reflecting the dominant first vortex shedding harmonic over an intermediate controlled attractor. Following our previous work,^{1,7,8,13} the global model will be a 3 states ODE, interpolating a single *shift state*, representing changes in the mean flow, and a pair of Fourier coefficients, reflecting the local von Karman expansion modes. The slowly varying shift state can also be used as the tuning parameter. Equivalent alternatives include the estimated instantaneous vortex shedding frequency or the low-pass filtered streamwise flow velocity at an equator point, in the near wake.

The advantage of the tuned model over the traditional POD model will be demonstrated both with respect to achievable closed loop performance and when sensor locations are optimized, to assure even performance throughout the transient range, rather than in a narrow neighborhood of the natural attractor.

II. The Cylinder Wake Benchmark, Design Objective and Basic Actuation

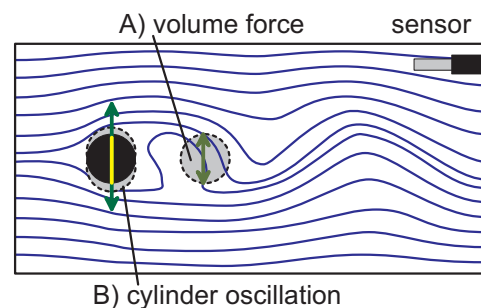


Figure 1. Principal sketch of the actuated cylinder wake. The cylinder is represented by the black disk. The location of the volume-force actuator (A) is indicated by a grey circle, and the transverse cylinder motion (B) by arrows. Streamlines represent the natural flow. The figure includes a hot-wire anemometer at a typical experimental position. This sensor has been used in an observer-based control using a Galerkin model¹.

The laminar two dimensional flow in the circular cylinder wake is used as a benchmark for the developments in this note. It is characterized by a transition to von Karman vortex shedding instability at $Re \approx 47$, and is considered here at $Re = 100$. The natural flow is then characterized by a periodic attractor. A common design objective¹⁴⁻¹⁷ in this system is to suppress this instability which causes mechanical vibrations and increased drag. Figure 1 provides a schematic of a postulated planar flow with two forms of actuation: The vertical volume-force actuator used in this note, which is supported over a downstream disk, and vertical vibrations of the disk, considered e.g. in^{2,18} and implemented experimentally at the Air Force Academy.⁷ Stream-lines represent the natural flow. The picture includes a hot-wire anemometer - a fluid velocity sensor - representing flow sensing, as previously discussed in.¹ Model-based optimization of sensor(s) position will be discussed in §F, as an example of a general framework for control hardware optimization and a demonstration of the advantage of the tuned models that are introduced in this note.

A simple, physically motivated control policy is to apply actuation as a dissipative deceleration force: The *energy extraction rate*

$$- \epsilon(t) \int_{\Omega} dV g(\mathbf{x}) \cdot \mathbf{u}(\mathbf{x}, t) \quad (1)$$

is approximately proportional to $-\epsilon(t)v_{vf}(t)$, where $v_{vf} = v(\mathbf{x}_{vf})$ is the vertical velocity field at the center of the supporting disk of the volume force, the point $\mathbf{x}_{vf} = (2D, 0)$, with D being the diameter of the cylinder and the radius support of the volume force. The amplitude of v_{vf} is denoted as \hat{v}_{vf} . The approximation gives rise to the feedback $\epsilon(t) = -k v_{vf}(t)$, where the gain $k > 0$ determines the dissipation rate. The purpose of the flow model, in this context, is to be able to approximate the value of $v_{vf}(t)$ from flow measurements. Under periodic vortex shedding, $v_{vf}(t)$ will be nearly periodic. Thus, a critical aspect of the predictive power of the model concerns the ability to infer the correct oscillation phase of $v_{vf}(t)$.

The simplified description of the flow as dominated by a nearly periodic vortex shedding is valid in the natural flow, as well as under low amplitude actuation at (about) the vortex shedding frequency, and as long as actuation does not attempt to significantly interfere with that frequency.¹ The respect of these restrictions is therefore a cornerstone of any effective design, including the developments in the paper. This will ensure, in particular, the validity of the modeling framework proposed here.

III. Empirical Control-oriented Galerkin Models

A. Control Design with POD of the Natural Flow

Starting point of the current efforts is the minimal Galerkin-model¹³ summarized in Appendix A. The Galerkin system is expressed in cylindrical coordinates:

$$\begin{bmatrix} \dot{r} \\ \dot{a}_3 \end{bmatrix} = \begin{bmatrix} \sigma_r & -\beta r \\ \delta r & -\rho \end{bmatrix} \begin{bmatrix} r \\ a_3 \end{bmatrix} + b \begin{bmatrix} \cos(\theta - \phi) \\ 0 \end{bmatrix} \epsilon + \begin{bmatrix} 0 \\ \eta_3 \end{bmatrix} \quad (2)$$

$$\dot{\phi} = \omega + \gamma a_3 + \frac{b}{r} \sin(\theta - \phi) \epsilon \quad (3)$$

where $\theta = \angle(g_1, g_2)$ and $b = \sqrt{g_1^2 + g_2^2}$. This form reveals two basic facts: First, *however designed*, an admissible actuation force that is effective in attenuating oscillations and that meets the constraint that the net period average impact on the oscillation frequency be negligible, must be in phase with $-\cos(\theta - \phi)$.^{1,4} This means that *any admissible control policy is bound to (roughly) immitate the simple physics based, dissipative policy suggested in §II*. A subsequent observation is that the angle θ , extracted from the low dimensional Galerkin approximation, is critical to correct orientation of the actuation force. This point will be revisited later.

A Galerkin model-based counterpart of the physics based policy of §II approximates $v_{vf}(t)$ by the vertical component of the Galerkin expansion (12), $a_1(t)\mathbf{u}_1(\mathbf{x}_{vf}) + a_2(t)\mathbf{u}_2(\mathbf{x}_{vf})$. Equivalently, the actuation is set to be proportional to $-r \cos(\theta - \phi)$. A dynamic observer, estimating this quantity from sensor measurements was developed in^{1,4} and a simplified variant is discussed in §D.

B. Interpolated POD Models

To understand the limitation on the effectiveness of the POD based control, right above, it is useful to consider Figure 2. The several plots in that figure are based on three sets of simulations, represented by the three rows: From top to bottom, those include the natural attractor and two controlled limit cycles, obtained by the dissipative control of §II with a moderate and a more aggressive feedback gains, applied directly to the correct value of v_{vf} . For each simulation the figure includes a snapshot of the flow field, from left to right, the mean flow field and the first oscillatory POD mode. While the topological characteristics of all three flow conditions are similar, they exhibit significant mutual deformations: The recirculation bubble is gradually elongated and the vortical structures are pushed downstream as the flow is stabilized. Particularly relevant here, are the changes in the values of $g_i = (\mathbf{u}_i, \mathbf{g})_{\Omega}$, hence in the critical value of the angle $\theta = \angle(g_1, g_2)$, and the definition of the flow phase $\phi(t) = \angle(a_1(t), a_2(t))$ in terms of the leading POD modes. When only the POD modes of the natural attractor are employed, both the value of θ and the definition of $\phi(t)$ that are used to determine the actuation signal become increasingly wrong as vortex shedding is attenuated. Eventually, these errors reach a level at which the actuation $\epsilon \propto -r \cos(\theta - \phi)$ is so out of phase that it loses its effectiveness.

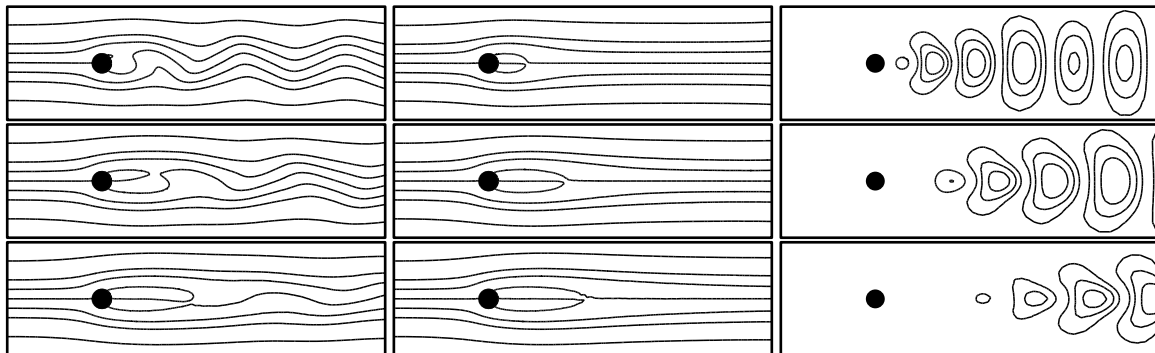


Figure 2. Left: Snapshots of level curves of the flow field; Middle: Averaged flows; Right: First POD mode. Top: the natural attractor; Middle: A moderately forced, attenuated attractor; Bottom: An aggressively actuated flow. Each row includes a snapshot the flow field (left), the mean flow field (middle) and the first oscillatory POD mode (right).

A model providing an effective solution to this problem must therefore account for the change in dominant modes along transients.²⁰ The solution suggested here exploits the structural similarity between controlled limit cycles, represented by the several lightly dotted circles in Figure 3. These orbits were obtained by complete information feedback $\epsilon = -kv_{vf}$, for escalated values of the gain k . Controlled transients with slow changes in the perturbation level progress along the manifold connecting these cycles. The dynamics near each of the cycles is dominated by the shift mode and two locally extracted oscillatory modes \mathbf{u}_1 and \mathbf{u}_2 . The Galerkin systems obtained by projecting the NSE (14) on these local modes are each of the form (17)-(3), albeit with different coefficients. The local values of the Galerkin system coefficients are functions of the characteristic value of a parameter representing the instantaneous flow condition. The Galerkin expansion will retain the form (17), with parameterized coefficients, and the expansion (12) will be interpreted with respect to the local expansion modes, associated with the present parameter value. This model will be valid for slow vertical transitions along the dynamic manifold in Figure 3 (which prevents the need to include the dynamics of mode deformation).

While the technical details of the interpolation deserve well more than the space available here, the key relevant fact for control design, in our system, is that the local model provides both the appropriate value of θ and appropriate local concepts of the instantaneous phase ϕ and amplitude r , of the flow. Indeed, these are the three key quantities needed for effective control.

C. Actuation Design With Interpolated Models

Again, a Galerkin model-based version of the dissipative feedback $\epsilon = -kv_{vf}$ of §II is that were $v_{vf}(t)$ is approximated by the the vertical component of the Galerkin expansion (12): $v_{vf}(t) \approx a_1(t)\mathbf{u}_1(\mathbf{x}_{vf}) + a_2(t)\mathbf{u}_2(\mathbf{x}_{vf})$. The difference from the implementation of §A is that now the tuned POD approximation is used. For Comparison a SISO phasor controller is implemented (see §D, E) that uses a sensor signal measured at $(x, y) = (3D, D)$. The amplitude for the feedback control is set such that it is the same as for the implementations above.

Figure 3 compares the natural attractor with limit cycles obtained by feedback control with a POD model extracted from the natural flow, control using the interpolated Galerkin model and, as a benchmark, control with direct flow measurement. In all cases, the feedback gain is identical: $k = 0.3$. It should be noted that with this gain complete attenuation cannot be achieved. As can be seen, the attenuation achieved with the traditional POD model is much inferior to what is attained with the interpolated model, which, in turn is close to the response with direct flow measurement.

In Table 1 several quantities are tabulated that show the performance of the standard model and the interpolated model. As in Figure 3 results for the natural flow, feedback control with a POD model extracted from the natural flow, control using the interpolated Galerkin model and control with direct flow measurement are shown. In addition results for a SISO simulation are shown that also uses an interpolated model. The SISO results compare well with the tuned POD. This improvement is enabled by the fact that the high level of flow reconstruction by the interpolated model is maintained along trajectories, but lost when just the

natural attractor's data is used.

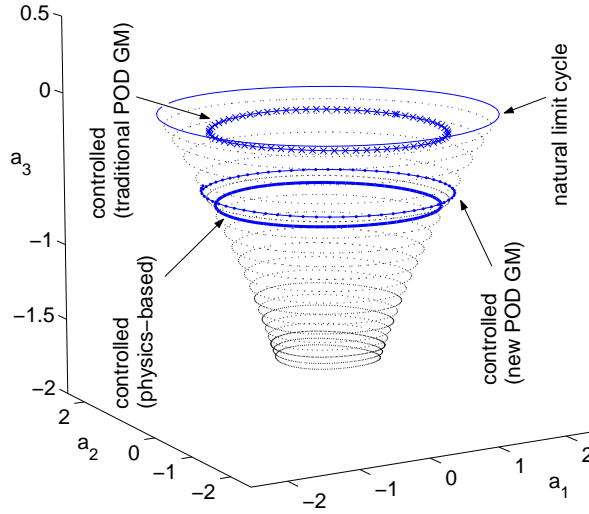


Figure 3. Phase Space of the first three Fourier coefficients a_1 , a_2 and a_3 , obtained by projection of the snapshots of the DNS data on the respective POD modes. The top limit cycle corresponds to the natural flow, the traditional POD GM corresponds to standard POD (using the natural flow data), the new POD GM is the interpolated model (using more reference simulations), and the physics-based control is feedback with direct flow measurements. All with feedback gain $\epsilon = -0.3v_{vf}$.

| | Natural Flow | Standard POD | Interpolated POD | SISO (see §E) | Complete Information |
|------------------|--------------|--------------|------------------|---------------|----------------------|
| $v_{vf \max}$ | 0.520 | 0.312 | 0.189 | 0.138 | 0.137 |
| x_{Rec} | 2.35 | 2.89 | 3.56 | 3.78 | 3.73 |
| TKE | 2.43 | 2.24 | 1.86 | 1.87 | 1.75 |
| a_3 | 0 | -0.17 | -0.47 | -0.71 | -0.67 |

Table 1. Quantities that highlight the differences between standard and interpolated models. The following quantities are tabulated: i) the oscillation amplitude of the vertical velocity v_{vf} at the point $(2D, 0)$, denoted $v_{vf \max}$, ii) the average length of the recirculation bubble x_{Rec} , iii) The perturbation (= turbulent kinetic) energy (TKE) in each limit cycle, and iv) the value of a_3 .

D. Observer Design with an Interpolated Model

A full state observer, based on the Galerkin system (15) in a fixed (no tuning) empirical GM is discussed in.^{1,4} Here we suggest a simpler alternative that, among other advantages, bypass the need to address the parameter and time dependence of expansion modes. Like the tuned model, the observer exploits the timescale separation between the periodic oscillations, represented schematically by motion in the horizontal cross sections of the manifold, in Figure 3, and the transition between operating points, represented by the vertical component of motion, in that figure. The latter is responsible, in particular, for slow changes in the oscillation frequency and amplitude.

For simplicity, we shall consider here the case of a single vertical velocity sensor at a point \mathbf{x}_s , although the ideas are extendable to the utilization of multiple sensors. The ideal sensor signal will be of the form

$$s = v_0(\mathbf{x}_s) + a_1 v_1(\mathbf{x}_s) + a_2 v_2(\mathbf{x}_s) = A_0 + A_1 \cos(\theta) + \text{noise}, \quad \dot{\theta} = \omega \quad (4)$$

where v_i are the vertical components of the vector-fields \mathbf{u}_i and parameter dependence notations are suppressed, where ω is interpreted as the instantaneous vortex shedding frequency (i.e., the quantity $\omega + \gamma a_3$ in (15)), and where both the unknown A_0 , A_1 and the frequency ω are slowly varying. Time variation will

be due to actuated changes in vortex shedding, and due to the associated changes in the dominant velocity fields.

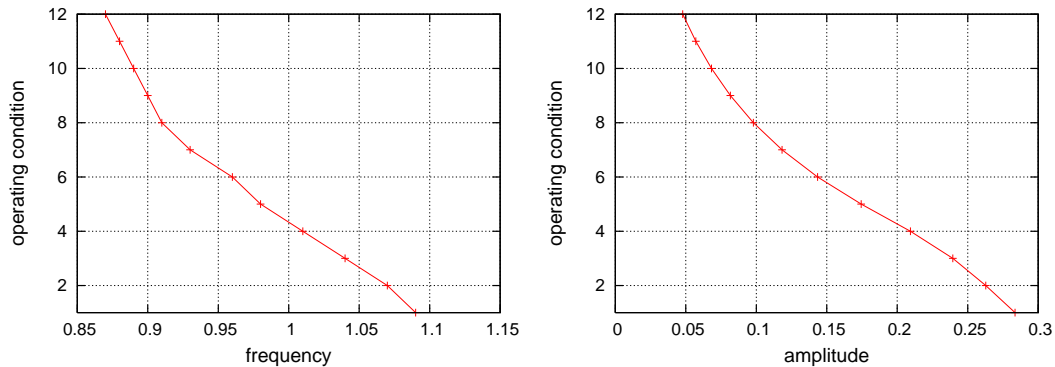


Figure 4. Parametrization of the operating condition. Left: Frequency as parameter. Right: Sensor amplitude as parameter.

The formulation (4) will be used to dynamically track slow changes in the coefficients A_0 , A_1 and the frequency ω and the nearly linear growth in θ as explained below. The estimated A_0 , A_1 and ω can be used to parameterize the tuned modes, see Figure 4 for an example.

The assumption that the quantities A_0 , A_1 , ω are subject to slow changes leads to a nominal discrete time dynamic model

$$\begin{bmatrix} A_0 \\ A_1 \\ \omega \\ \theta \end{bmatrix} (t_{k+1}) = \begin{bmatrix} 1 & 0 & 0 & 0 \\ 0 & 1 & 0 & 0 \\ 0 & 0 & 1 & 0 \\ 0 & 0 & \Delta t & 1 \end{bmatrix} \begin{bmatrix} A_0 \\ A_1 \\ \omega \\ \theta \end{bmatrix} (t_k) \quad (5)$$

$$s(t_k) = A_0(t_k) + A_1(t_k) \cos(\theta(t_k)) \quad (6)$$

where Δt is the time step. This framework is, in fact, a simpler variant of the dynamic phasor approximation used in,²¹ and readily lends itself to state estimation by an extended Kalman filter (EKF), where the emphasis is on conservative, hence slow tracking.

Model eq. 5, 6 forms a (slow) narrow banded low-pass filter for reconstruction of the sensor signal. The plots in Figure 5 demonstrate the dynamic reconstruction of the sensor signal for a sensor at $(x, y) = (3D, D)$. The zoom on the left side in Figure 5 shows that the observer lags approximately one period behind the sensor signal during relatively fast transients, i.e. the model assumption 5 is not adequate here.

The position of the single velocity sensor can be optimized, as described in §F, below.

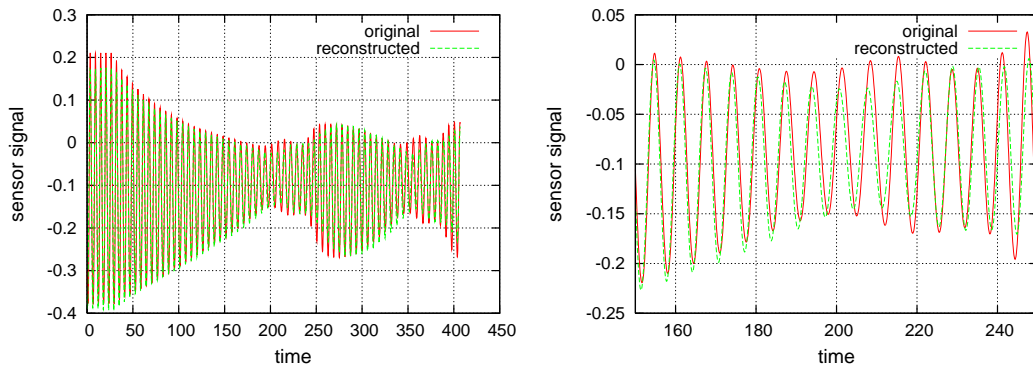


Figure 5. Plot of the sensed velocity trajectory and its dynamic estimate. Both the entire trajectory and a zoom on a fast changing transient are displayed.

E. SISO Control With Interpolated Models

As noted before the only admissible control policy is the physics based, dissipative policy described in §II. The optimal actuation is based on the energy extraction rate; eq. 1: $-\epsilon(t) \int_{\Omega} dV g(\mathbf{x}) \cdot \mathbf{u}(\mathbf{x}, t)$

The goal here is to relate the ideal actuation signal 1 to the dynamically estimated signal 6. Therefore eq. 1 is written as follows:

$$-\epsilon(t) \int_{\Omega} dV g(\mathbf{x}) \cdot \mathbf{u}(\mathbf{x}, t) = -k(t) \cos(\theta_s(t) + \Delta\phi(t)) \quad (7)$$

where k is the amplitude of the volume force, θ_s the phase of the sensor signal and $\Delta\phi$ the phase difference between the sensor signal and the ideal actuation signal (i.e. the phase of the projection on the left hand side of the equation). For a sensor at $(x, y) = (3D, D)$, where D is the cylinder diameter, the phase difference $\Delta\phi$ as function of the sensor amplitude is shown in Figure 6. Note that the sensor used here is optimal in the sense that the changes in phase difference are small over the simulated trajectories (about 10°).

The dynamic observer estimates the frequency and leading phasors of the sensor signal. A lookup table is then used to determine the phase difference between the sensor signal and ideal actuation.

An example of SISO sensor feedback is shown in Figure 7. Here the amplitude of the volume force k and the velocity signal at the center of the volume force $v_{v,f}$ (an approximation to the projection) are plotted. Ideally these two signals should be 180° out of phase all the time. The goal in this simulation was to stabilize the flow at a fluctuation level that corresponds to an amplitude $\hat{v}_{v,f} \approx 0.07$ (time ≈ 200). The fluctuation level is decreased to the desired level, rises to a well defined fluctuation level and drops again to the desired level and so on. This pattern is confirmed by simulations similar to the one shown in Figure 7.

As shown in previous work⁸ for a similar configuration where the wake is suppressed using a translating cylinder instead of a volume force, there are stable and unstable limit cycles under closed loop control. We believe that this is the case here. The fluctuation level is brought down to the desired level, but since this level corresponds to an unstable limit cycle it is not possible to maintain the flow there (at least under the control policy used here). Hence the fluctuation level rises to a level that corresponds to a stable limit cycle under closed loop control.

This conjecture is illustrated in a second simulation where the same control law is used as before. The control goal is to stabilize the flow at a fluctuation level that corresponds to an amplitude $\hat{v}_{v,f} \approx 0.24$. Here the amplitude settles at a steady level and no ‘ringing effects’ are observed. The amplitude of the volume force k and the velocity signal at the center of the volume force $v_{v,f}$ of this simulation are shown in Figure 8.

In Figure 9 the recirculation length of the two discussed simulations are compared with each other. The recirculation length, defined as the point where the downstream velocity changes sign on the equator, gives a good indication of the change in mean flow. The ringing phenomenon as shown in Figure 7, corresponding to problems in phase estimation, can be directly observed (s1). The stabilized wake, characterized by a higher fluctuation level, corresponds to the steady lower recirculation length (s2).

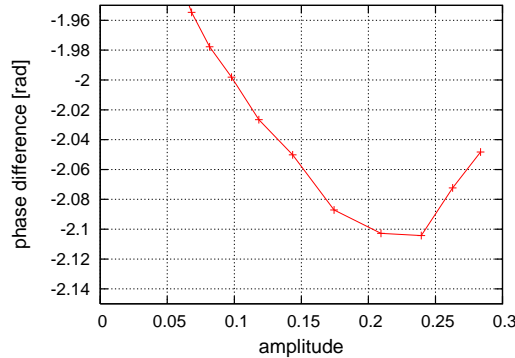


Figure 6. The phase difference $\Delta\phi$ between the sensor signal and the ideal actuation signal as function of the sensor amplitude A_1 at location $(x, y) = (3D, D)$.

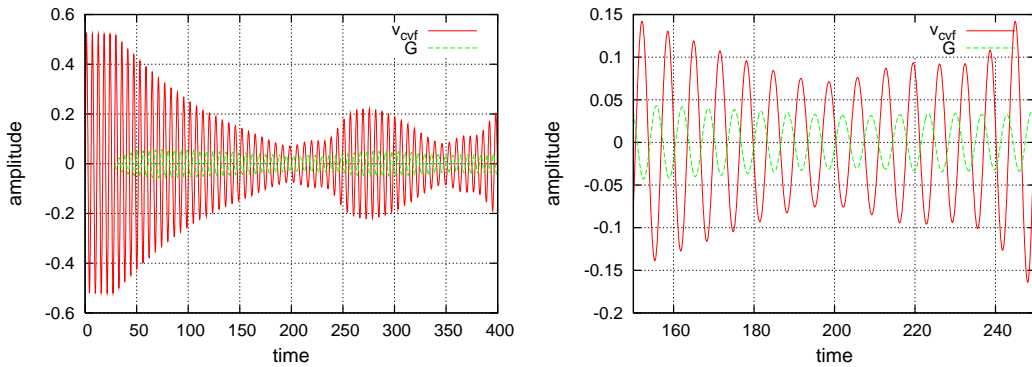


Figure 7. Plot of the amplitude of the volume force and the velocity at the center of the volume force vs. time. The control goal is to reduce the fluctuation level of the flow corresponding to an amplitude $\hat{v}_{vf} \approx 0.07$. The zoom illustrates the phase problem around the desired state.

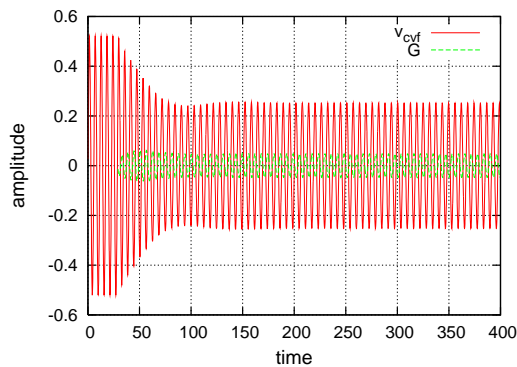


Figure 8. Plot of the amplitude of the volume force and the velocity at the center of the volume force vs. time. The control goal is to reduce the fluctuation level of the flow corresponding to an amplitude $\hat{v}_{vf} \approx 0.24$.

F. Optimizing Sensor Location and Observation with an Interpolated POD Model

The tradeoff between cost, hardware constraints and performance, a hallmark of control engineering, becomes critical in fluid flow applications. Indeed, limitations on feasible locations, weight and size of actuation and sensing hardware clearly makes the efficiency of that hardware a make-or-brake issue. Here we discuss the utility of tuned GMs as a basis for a systematic framework to asses and optimize hardware placement, and

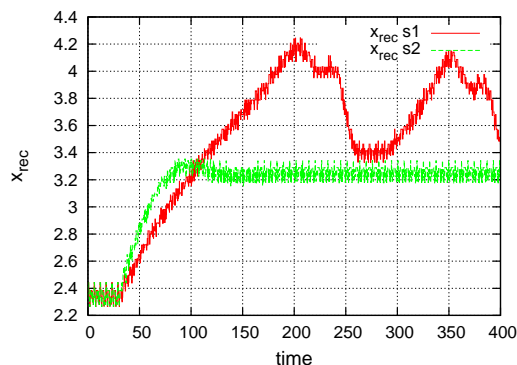


Figure 9. The elongation of the recirculation length as a function of time. The legend s1 refers to the simulation shown in Figure 7. and the legend s2 refers to the simulation shown in Figure 8.

illustrate that framework in the context of optimized sensor(s) location in the cylinder wake benchmark.

The inverted observability and controllability Grammians of linear (time varying) systems define measures of the required actuation effort and the sensitivity of an output signal to state changes. The smallest singular values of the respective Grammians therefore provide systematic quantification of the dynamic effectiveness of sensors and actuators²² and yield meaningful cost indices for model based optimization. In a nonlinear system, Grammians defined by linearizations along representative trajectories are the natural substitute. When the system is nearly periodic, the Grammians associated with a single period and normalized by the period length are natural candidates. As may well be expected and as is illustrated in the cylinder wake flow, below, changes in dominant modes as the system transitions between operating points are reflected by changes in the sensitivity of sensors to state dynamics. A meaningful optimization criterion would therefore be to maximize the worst sensor performance over the entire transient range.

Consider now the cylinder wake flow with a finite set of sensors. For notational simplicity we shall assume that all these sensors measure the vertical velocity (i.e., the “ v ” component of the velocity field) at points \mathbf{x}_k , $k = 1 : \dots, K$. We shall focus on the short term sensitivity of the sensor to the phase and amplitude of the Fourier coefficients a_1 and a_2 . In a simplified continuous time model one can thus assume a fixed frequency. Invoking the appropriately adjusted notations of (4) and denoting the model tuning parameter by “ p ” (e.g., $p = \omega$), the sensing problem is defined in the system

$$\frac{d}{dt} \begin{bmatrix} a_1 \\ a_2 \end{bmatrix} = A(p) \begin{bmatrix} a_1 \\ a_2 \end{bmatrix}, \quad s_{hp} := s - A_0 = C(\bar{\mathbf{x}}, p) \begin{bmatrix} a_1 \\ a_2 \end{bmatrix} \quad (8)$$

where $\bar{\mathbf{x}} = \{\mathbf{x}_k, k = 1 : \dots, K\}$ and where

$$A(p) = \begin{bmatrix} 0 & -\omega \\ \omega & 0 \end{bmatrix} \quad \text{and} \quad C(\bar{\mathbf{x}}, p) = \begin{bmatrix} v_1(\mathbf{x}_1, p) & v_2(\mathbf{x}_1, p) \\ v_1(\mathbf{x}_2, p) & v_2(\mathbf{x}_2, p) \\ \vdots & \vdots \\ v_1(\mathbf{x}_K, p) & v_2(\mathbf{x}_K, p) \end{bmatrix} \quad (9)$$

It is easy to see that the normalized single period observability Grammian is, in this case

$$\frac{1}{T} G_o(T, \bar{\mathbf{x}}, p) = \frac{1}{T} \int_0^T e^{A(p)'t} C(\bar{\mathbf{x}}, p)' C(\bar{\mathbf{x}}, p) e^{A(p)t} dt = 0.5 \|C(\bar{\mathbf{x}}, p)\|_F^2 \quad (10)$$

where we use the explicit form of the matrix exponential, the subscript F indicates the Frobenius norm, and I_2 is the 2×2 identity. The optimal sensor location is therefore determined as the solution of the optimization problem

$$\max_{\bar{\mathbf{x}}} \min_p \|C(\bar{\mathbf{x}}, p)\|_F \quad (11)$$

In Figure 10 we show plots of $\|C(\bar{\mathbf{x}}, p)\|_F$ as a function of p , where the set of sensor locations $\bar{\mathbf{x}}_*$ was optimized with respect to the first 1, 4, 9 or 18 (out of 18) equally spaced operating conditions, for both a single and for three velocity sensors. As is clearly observed, the predicted performance of sensors that are optimized for a single parameter value (i.e., for the natural attractor) is higher early on but deteriorates rapidly with the change of p , while those optimized over a wider range maintain an increasingly even performance during transitions. Multiple sensors improve both the relative flatness (peak-to-peak ratio) of this performance measure and increase the minimal value.

IV. Conclusions

A framework of interpolated Galerkin models for fluid flow systems strikes a balance between the need for higher number of modes to represent actuation and transients and the desire to maintain model simplicity and minimize the number of dynamic variables that need to be estimated in real time, in feedback implementation. Advantages over traditional POD models have been illustrated in the context of vortex shedding suppression behind a circular cylinder, and are manifest by improved ability to suppress vortex shedding and an improved sensor performance over a wider transients range. Due to intrinsic instabilities it is difficult to fully stabilize the wake using SISO control with interpolated models.

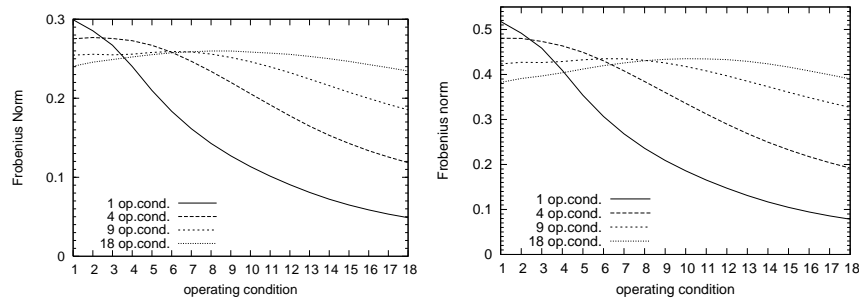


Figure 10. Plots of the Frobenius norm $\|C(\bar{x}_*, p)\|_F$ as a function of the operating condition p for a single sensor (left) and 3 sensors (right). The optimal sensor location(s) vector \bar{x}_* is computed for the first 1, 4, 9 or 18 (out of 18) equally spaced operating points.

Acknowledgments

We acknowledge funding from the Deutsche Forschungsgemeinschaft (DFG) and the U.S. National Science Foundation (NSF). DFG support was via the Collaborative Research Center (Sfb 557) "Control of complex turbulent shear flows" at the Berlin University of Technology and by grants NO 258/1-1 and DI 448/5-1. NSF support was via grants No. 0136404, 0410246 and 0230489.

References

- ¹J. Gerhard, M. Pastoor, R. King, B.R. Noack, A. Dillmann, M. Morzyński & G. Tadmor, Model-based control of vortex shedding using low-dimensional Galerkin models, *AIAA-Paper 2003-4261*, 33rd AIAA Fluid Dynamics Conference and Exhibit, 2003.
- ²K. Cohen, S. Siegel, T. McLaughlin, and J. Myatt. Proper orthogonal decomposition modeling of a controlled Ginzburg-Landau cylinder wake model, *AIAA-Paper 2003-1292*, 41st Aerospace Sciences Meeting and Exhibit, 2003.
- ³S. Siegel, K. Cohen & T. McLaughlin. Feedback Control of a Circular Cylinder Wake in Experiment and Simulation, *AIAA-Paper 2003-3571*, 33rd AIAA Fluids Conference and Exhibit, 2003.
- ⁴G. Tadmor, B.R. Noack, A. Dillmann, J. Gerhard, M. Pastoor, R. King, and M. Morzyński. Control, observation and energy regulation of wake flow instabilities, *42nd IEEE Conference on Decision and Control*, pages 2334–2339, 2003.
- ⁵C.W. Rowley, T. Colonius, and R.M. Murray. Model reduction for compressible flows using POD and Galerkin projection. *Physica D*, 189:115–129, 2004.
- ⁶K. Cohen, S. Siegel, M. Luchtenburg, T. McLaughlin, and A. Seifert. Sensor placement for closed-loop flow control of a 'D' shaped cylinder wake, *AIAA Paper 2004-2523*, 2nd AIAA Flow Control Conference, 2004.
- ⁷B.R. Noack, G. Tadmor, and M. Morzyński. Low-dimensional models for feedback flow control. Part I: Empirical Galerkin models, *AIAA Paper 2004-2408*, 2nd AIAA Flow Control Conference, 2004.
- ⁸G. Tadmor, B.R. Noack, M. Morzyński, and S. Siegel. Low-dimensional models for feedback flow control. Part II: Controller design and dynamic estimation, *AIAA Paper 2004-2409*, 2nd AIAA Flow Control Conference, 2004.
- ⁹M. Bergmann, L. Cordier, and J.-P. Brancher. Optimal rotary control of the cylinder wake using POD reduced order model. *AIAA Paper 2004-2323*, 2nd AIAA Flow Control Conference, 2004.
- ¹⁰C.W. Rowley. Model reduction for fluids, using balanced proper orthogonal decomposition, *Int. J. on Bifurcation and Chaos*, 2005. in press.
- ¹¹R. King, M. Seibold, O. Lehmann, B.R. Noack, M. Morzyński and G. Tadmor. Nonlinear flow control based on a low dimensional model of fluid flow in Control and Observer Design for Nonlinear Finite and Infinite Dimensional Systems, T. Meurer, K. Graichen and E.D. Gilles (Editors). *Lecture notes in Control & Information Science Volume 322*, pp. 369-386, Springer, 2005.
- ¹²P. Holmes, J.L. Lumley, and G. Berkooz. *Turbulence, Coherent Structures, Dynamical Systems and Symmetry*. Cambridge University Press, 1998.
- ¹³B.R. Noack, K. Afanasiev, M. Morzyński, G. Tadmor, and F. Thiele. A hierarchy of low-dimensional models for the transient and post-transient cylinder wake. *J. Fluid Mech.*, 497:335–363, 2003.
- ¹⁴M. F. Unal and D. Rockwell. On the vortex formation from a cylinder; Part 2. control by a splitter-plate interference. *J. Fluid Mech.*, 190:513–529, 1987.
- ¹⁵P. J. Strykowski and K. R. Sreenivasan. On the formation and suppression of vortex shedding at low Reynolds numbers. *J. Fluid Mech.*, 218, 1990.
- ¹⁶E. Detemple-Laake and H. Eckelmann. Phenomenology of Kármán vortex streets in oscillatory flow. *Exps. Fluids*, 7:217–227, 1989.
- ¹⁷K. Roussopoulos. Feedback control of vortex shedding at low Reynolds numbers. *J. Fluid Mech.*, 248:267–296, 1993.
- ¹⁸B.R. Noack, G. Tadmor, and M. Morzyński. Actuation models and dissipative control in empirical Galerkin models of fluid flows. In *The 2004 American Control Conference*, Boston, MA, U.S.A., June 30–July 2, 2004. Paper **FrP15.6**.
- ¹⁹B.R. Noack, P. Papas, and P.A. Monkewitz. The need for a pressure-term representation in empirical Galerkin models of incompressible shear flows. *J. Fluid Mech.*, 523:339–365, 2005.

²⁰O. Lehmann, M. Luchtenburg, B.R. Noack, R. King, M. Morzyński and G. Tadmor Wake stabilization using POD Galerkin models with interpolated modes *44th IEEE Conference on Decision and Control and European Control Conference ECC*, Seville, Spain, 12–15 December 2005.

²¹G. Tadmor. Observers and feedback control for a rotating vortex pair. *IEEE Transactions on Control Systems Technology*, 12:36 – 51, 2004.

²²K. B. Lim. Method for optimal actuator and sensor placement for large flexible structures. *J. Guidance, Cont. Dyn.*, 15:49–57, 1992.

A. Empirical Galerkin Models

A. Basic Framework

Galerkin models (GMs) are based on an approximation of the flow’s velocity field as a combination of a base flow (say, the natural mean flow) and an orthonormal mode set

$$\mathbf{u}^{[N]} = \sum_{i=0}^N a_i(t) \mathbf{u}_i(\mathbf{x}), \quad (12)$$

where \mathbf{u}_0 is a base mode with amplitude $a_1 = 1$.

The time invariant modes $\mathbf{u}_i(\mathbf{x})$ satisfy the boundary conditions and non-compressibility conditions (when applied) and are embedded in the spatial \mathcal{L}_2 space, including the inner product

$$(\mathbf{u}, \mathbf{v})_{\Omega} := \int_{\Omega} dV \mathbf{u} \cdot \mathbf{v}, \quad \mathbf{u}, \mathbf{v} \in \mathcal{L}_2(\Omega). \quad (13)$$

Time dependence is restricted to the Fourier coefficients $a_i(t)$. Time dynamics are derived from the non-dimensionalized, Navier-Stokes equation (NSE)

$$\partial_t \mathbf{u} + \nabla \cdot (\mathbf{u}\mathbf{u}) = -\nabla p + \frac{1}{Re} \Delta \mathbf{u} + \epsilon \mathbf{g}, \quad \nabla \cdot \mathbf{u} = 0 \quad (14)$$

where \mathbf{x} represents location, t is time, \mathbf{u} the velocity field, p , the pressure, \mathbf{g} is a volume force modulated by the commanded amplitude ϵ , representing the control mechanism considered in this note. A compression of (14) to the subspace spanned by the selected modes yields a quadratically nonlinear ordinary differential equation, termed the Galerkin system

$$\frac{d}{dt} a_i = \frac{1}{Re} \sum_{j=0}^N l_{ij} a_j + \sum_{j,k=0}^N q_{ijk} a_j a_k + \epsilon \mathbf{g}_i \quad \text{for } i = 1, \dots, N, \quad (15)$$

where the linear and quadratic terms represent the viscous and convective Navier-Stokes terms, respectively, with constant coefficients $l_{ij} := (\mathbf{u}_i, \Delta \mathbf{u}_j)_{\Omega}$, $q_{ijk} := (\mathbf{u}_i, \nabla \cdot (\mathbf{u}_j, \mathbf{u}_k))_{\Omega}$ and $\mathbf{g}_i := (\mathbf{u}_i, \mathbf{g})_{\Omega}$ the projection of the volume force. In particular, the coefficients of (14) are commonly obtained by a projection (known as the Galerkin projection) of the right hand side of (14) on the modes subspace. In very low order approximations, the Galerkin projection may lead to dynamic distortions, resulting from neglected domain and signal space components, including a truncated energy cascade and neglected net pressure work. Estimation methods^{7,19} can be used to improve model fidelity, adjusting the values of coefficients in (15) but maintaining its form.

In proper orthogonal decomposition¹² approximations, \mathbf{u}_i , $i = 1, \dots, N$, are Karhunen-Loève modes, obtained from experimental data or from a numerical simulation of (14) as linear combinations of fluctuation snapshots $\mathbf{u}^m - \mathbf{u}_0$, $m = 1, \dots, M$, $M \gg N$, of a reference trajectory. The chosen combinations minimize the averaged energy residual of the Galerkin ansatz (12) with respect to the snapshot ensemble. In this respect, (12) is then an optimal *kinematic* approximation of the reference.

The efficiency of the POD approximation often comes at the cost of fragility, away from the reference trajectory. The Galerkin approximation is hardwired to the actuation used at the reference and the Galerkin system does not accommodate dynamics associated with other actuation inputs or initial data. In particular, the system does not include dynamically significant modes that are orthogonal to the subspace spanned by the reference, such as changes in the mean flow. As a first step to address this issue the authors have elaborated the role of the shift-mode^{7,1} as an enabler for non-equilibrium model for transient flow. The shift-mode \mathbf{u}_{Δ} represents mean-field correction and is aligned with the difference between the unstable steady Navier-Stokes

solution \mathbf{u}_s and the time-averaged flow \mathbf{u}_0 . Formally, the shift-mode \mathbf{u}_Δ and its amplitude a_Δ are considered as the $N + 1^{st}$ mode and Fourier coefficient, respectively. As shown in,^{2,1,4} the inclusion of the shift mode leads to a dramatic improvement in the dynamic predictive power of the model.

Volume force actuation is chosen here as a simple control mechanism. It may physically represent a Lorentz force in magneto-hydrodynamical flows, a simplified formulation of a plasma actuator, a buoyancy term in the Boussinesq approximation, or an external pressure gradient in pipe flows. This actuation is represented by a control term of the form ϵg_i on the right-hand side of the i^{th} Galerkin system equation (15), where $g_i := (\mathbf{u}_i, \mathbf{g})_\Omega$ is the time-invariant amplitude of the projection of the volume force field \mathbf{g} on \mathbf{u}_i . Alternative forcing may involve state dependent g_i coefficients and require the inclusion of actuation modes⁷ in the Galerkin expansion (12).

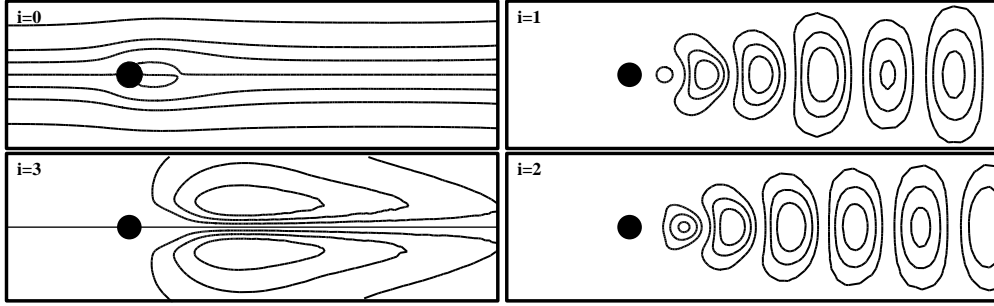


Figure 11. Expansion modes, visualized by streamlines, derived from the natural attractor. In clockwise order: the mean flow ($i = 0$), the first two POD modes ($i = 1, 2$) resolving 95% of the fluctuation energy at the reference simulation, and the shift mode ($i = 3$).

B. Application to the Controlled Cylinder Wake

The natural attractor is dominated by the first harmonic of the periodic vortex shedding, represented by modes \mathbf{u}_1 and \mathbf{u}_2 in Figure 11. These modes capture some 95% of the perturbation energy over the attractor. The mean flow \mathbf{u}_0 and the unstable, steady flow \mathbf{u}_s , shown in that figure, are structurally similar, and are characterized by symmetry with respect to the x axis and a recirculation bubble in the near wake. The transition to the attractor is characterized by a shortened recirculation bubble. The normalized difference $\mathbf{u}_0 - \mathbf{u}_s$ is the shift mode $\mathbf{u}_\Delta = \mathbf{u}_3$. (Thus the Fourier coefficient value $a_3 = 0$ represents the attractor^a.) A Galerkin system, based on these 3 modes is of the form

$$\dot{a} = A(a)a + B\epsilon + \eta, \quad s = Ca \quad (16)$$

where $a := [a_1, a_2, a_3]^T$, $\eta = [0, 0, \eta_3]^T$ is the constant term from (15), ϵ is the actuation command, s is the sensor reading, and

$$A(a) := \begin{bmatrix} \sigma_r & -(\omega + \gamma a_3) & -\beta a_1 \\ (\omega + \gamma a_3) & \sigma_r & -\beta a_2 \\ \delta a_1 & \delta a_2 & -\rho \end{bmatrix}, \quad B = \begin{bmatrix} g_1 \\ g_2 \\ 0 \end{bmatrix} \quad (17)$$

The sensor coefficient for a single sensor is $C = [c_1, c_2, c_3]$. With multiple sensors, the matrix C will comprise several rows of a similar form.

Dynamic features are transparent from this model, including a periodic attractor and a nearly parabolic attractive invariant manifold of transients from perturbations of the steady solution ($a_1 = a_2 = 0$) to the attractor ($a_3 = 0$), in the unactuated flow.^{?,?}

Key aspects of actuation restrictions are clarified when (17) is expressed in cylindrical coordinates

$$\begin{bmatrix} a_1 \\ a_2 \end{bmatrix} = r \begin{bmatrix} \cos(\phi) \\ \sin(\phi) \end{bmatrix} \quad (18)$$

with r^2 indicating the fluctuation level, and ϕ the flow phase.

^aThe convention that $a_3 = 0$ on the attractor is different from some of our previous notes, and results here with $\sigma_r \approx 0$.